SCIENTIFIC REPORTS

OPEN

Novel nanowire-structured polypyrrole-cobalt composite as efficient catalyst for oxygen reduction reaction

Received: 09 November 2015
Accepted: 22 December 2015
Published: 10 February 2016

Xianxia Yuan[1], Lin Li[1], Zhong Ma[1], Xuebin Yu[2], Xiufang Wen[3], Zi-Feng Ma[1], Lei Zhang[4], David P. Wilkinson[5] & Jiujun Zhang[4]

A novel nanowire-structured polypyrrole-cobalt composite, PPy-CTAB-Co, is successfully synthesized with a surfactant of cetyltrimethylammounium bromide (CTAB). As an electro-catalyst towards oxygen reduction reaction (ORR) in alkaline media, this PPy-CTAB-Co demonstrates a superior ORR performance when compared to that of granular PPy-Co catalyst and also a much better durability than the commercial 20 wt% Pt/C catalyst. Physiochemical characterization indicates that the enhanced ORR performance of the nanowire PPy-CTAB-Co can be attributed to the high quantity of Co-pyridinic-N groups as ORR active sites and its large specific surface area which allows to expose more active sites for facilitating oxygen reduction reaction. It is expected this PPy-CTAB-Co would be a good candidate for alkaline fuel cell cathode catalyst.

Polymer electrolyte membrane Fuel cells (PEMFCs) are a kind of prospective green power sources that can convert chemical energy in the fuel directly into electricity with high energy efficiency and low/zero emissions[1–4]. Their performance including energy/power densities and life-time strongly depends on the electrocatalysts for promoting the oxygen reduction reaction (ORR) at cathode. At current state of technology, platinum- and its alloys-based materials are the most efficient and practical ORR catalysts which can give both high electrochemical activity and acceptable durability. However, the scarcity of platinum and its high cost limit fuel cells' wide and sustainable commercialization.

Currently, there are two major types of PEMFCs, one is the proton exchange membrane fuel cells (also called Acid-PEMFCs) where the membranes are proton conductive, and the other is the Alkaline-PEMFCs where the membranes are hydroxide conductive. In normal, due to the acidic environment of Acid-PEMFCs, their cathode ORR is slower than that in Alkaline-PEMFCs. Thus, Alkaline-PEMFCs may present more opportunities for non-Pt–based electrocatalysts for ORR than that Acid-PEMFCs do. In this sense, Alkaline-PEMFCs are considered to be the feasible and promising alternatives to Acid-PEMFCs in terms of their possible usage of non-noble metal catalysts as well as their better stability of component materials than that in Acid-PEMFCs[5–7].

Regarding non-noble metal catalysts for PEMFC applications, a wide range of catalyst materials have been explored in the last several decades, including transition metal macrocycles[8–10], manganese oxides[11–13], spinel AB_2O_4 complexes[14–16], heat-treated carbon supported transition metal-nitrogen complexes (M-N/C, M = Fe, Co, Mn, etc.)[17–19], perovskite-type oxides[20–22] and metal free catalysts[23–25]. Among them, the M-N/C catalysts have been paid great attentions owing to their higher activities and four-electron-transfer selectivity towards ORR. As a representative member of M-N/C catalysts, polypyrrole (PPy)-based cobalt-contained catalyst has been investigated in recent years as ORR catalyst in alkaline media and demonstrated promising performance[26,27]. Even the metal free pristine PPy and pyrolyzed PPy have also been investigated as ORR catalysts in acidic solutions[28,29]. Depending on the preparation conditions, PPy could be formed into various morphologies[30], such as film[31],

[1]Department of Chemical Engineering, Shanghai Jiao Tong University, Shanghai, 200240, China. [2]Department of Materials Science, Fudan University, Shanghai, 200433, China. [3]The School of Chemistry and Chemical Engineering, South China University of Technology, Guangzhou, 510640, China. [4]Energy, Mining & Environment, National Research Council of Canada, Vancouver, BC V6T 1W5, Canada. [5]Department of Chemical and Biochemical Engineering, University of British Columbia, Vancouver, Canada. Correspondence and requests for materials should be addressed to X.Y. (email: yuanxx@sjtu.edu.cn)

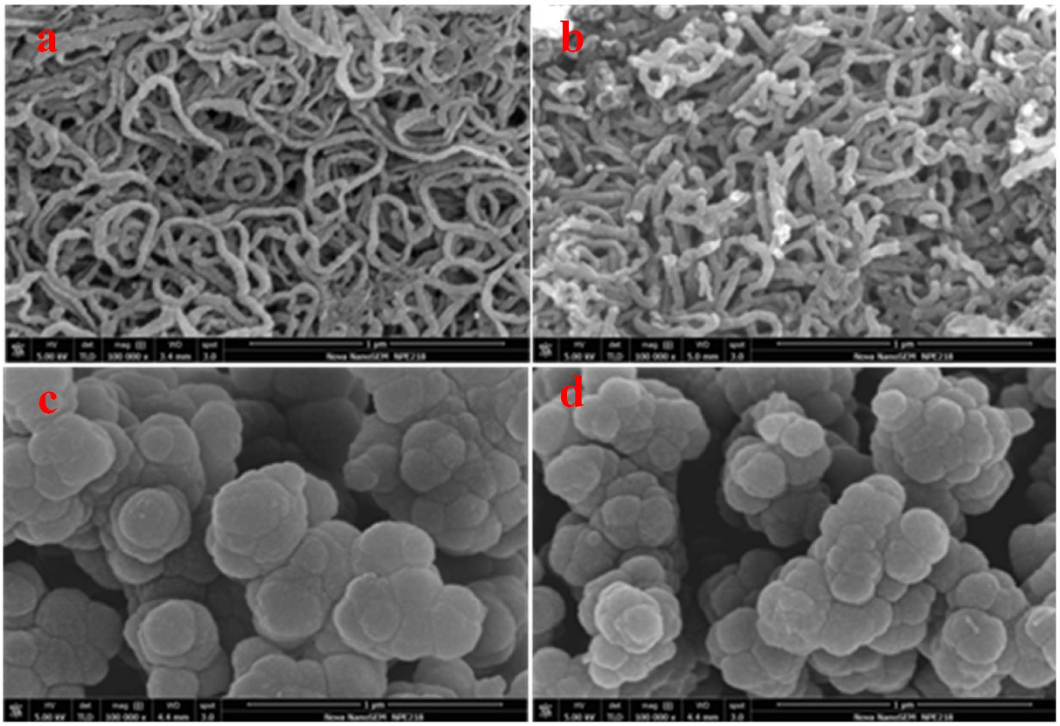

Figure 1. SEM images of PPy-CTAB (**a**), PPy-CTAB-Co (**b**), PPy (**c**), and PPy-Co (**d**).

nanoparticle[32], nanotube array[33], nanowire[34,35], microtube[36], hollow structure[37] and so on. The morphology of PPy has been identified to influence its ORR performance as the metal free catalyst. Morozan *et al.*[38] reported that pyrolyzed PPy with tubules-like morphology could exhibit a much better ORR catalytic performance in 0.1 M KOH than that with granular-like morphology. However, the morphology effects of metal-contained PPy catalysts on their ORR performance in either alkaline or acidic media have seldom been seen in literature.

In this work, a nanowire-structured PPy-Cobalt composite was synthesized using nanowire polypyrrole and cobalt acetate by surface immobilization of cobalt ions followed by a pyrolysis in an inert atmosphere, its ORR performance in alkaline solution was electrochemically evaluated and compared with that of the PPy-Co granules. Experiment results showed that this novel catalyst had a superior ORR performance compared to a granular PPy-Co catalyst and also a better durability than commercial 20% Pt/C catalyst. To understand the enhancement effect of this catalyst for ORR, some physiochemical characterizations, including X-ray diffraction (XRD), scanning electron microscopy (SEM), transmission electron microscopy (TEM), X-ray photoelectron spectroscopy (XPS), N_2 adsorption-desorption isotherm and Inductive Coupled Plasma Emission Spectrometer (ICP), were employed. It is concluded that the ORR enhancement effect of such a catalyst is due to the resulted Co-pyridinic-N active sites for ORR and also a larger specific surface area with more active site exposure.

Results

Synthesis and characterization of catalysts. SEM images were taken to observe morphologies of the as-prepared polypyrrole and the cobalt-anchored catalysts. Figure 1a identifies nanowire morphology of the PPy-CTAB prepared with CTAB as the surfactant, its nanowire structure can still be maintained after the addition of Co metal and the pyrolysis process, as shown in Fig. 1b for the PPy-CTAB-Co catalyst. However, the average nanowire size was slightly increased probably owing to the agglomeration of nanowire PPy during the pyrolysis. In contrast, a granular morphology can be observed for both PPy (Fig. 1c) which was prepared without surfactant and the cobalt-contained catalyst of PPy-Co (Fig. 1d), but the average size of the PPy-Co catalyst is slightly smaller, which could be ascribed to the decomposition of PPy and the structure re-configuration during the pyrolysis. Both the nanowire and granular structures of PPy-CTAB-Co and PPy-Co catalysts could also be observed with the TEM images (Fig. 2).

Electrochemical performance of the catalysts towards ORR. The catalytic ORR activity of the nanowire-structured PPy-CTAB-Co was evaluated in O_2-saturated 0.1 M KOH electrolyte with CV in a three-electrode cell at 5 mV s^{-1}, the obtained result is shown in Fig. 3a, where the CV curves of both PPy-Co granules and 20 wt% Pt/C catalysts are also shown for comparison. Although the ORR activities of both nanowire PPy-CTAB-Co and granular PPy-Co catalysts are apparently lower than that of 20 wt% Pt/C catalyst as seen from the ORR peak potentials, the activity of PPy-CTAB-Co is, however, significantly higher than that of PPy-Co. Its ORR peak at about −0.182 V is apparently more positive than that of −0.213 V for the granular PPy-Co. Moreover, the ORR peak current density of PPy-CTAB-Co is about twice higher than that for PPy-Co. These results imply the higher ORR catalytic activity of nanowire PPy-CTAB-Co than granular PPy-Co catalyst.

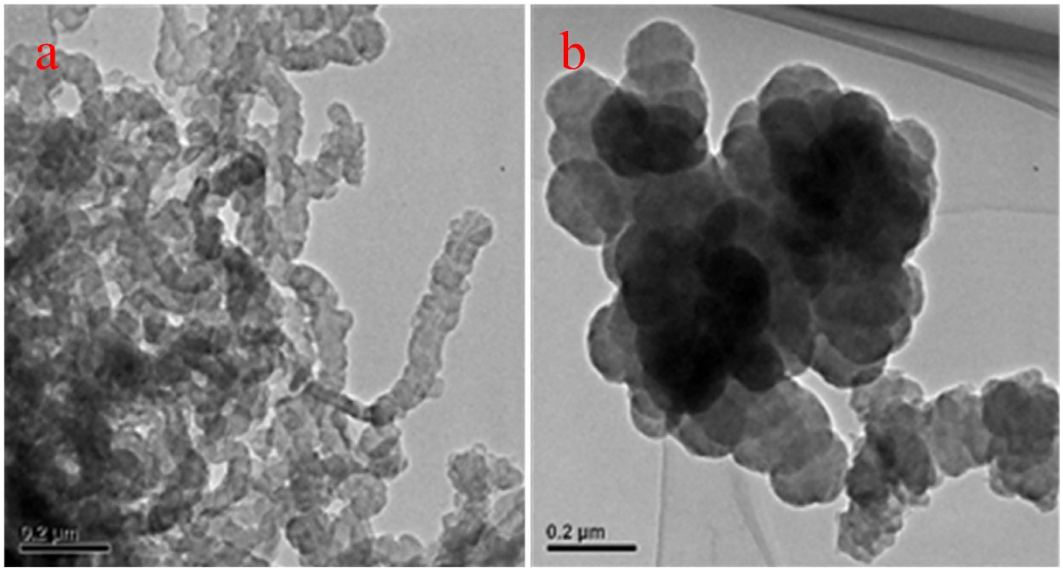

Figure 2. TEM images of PPy-CTAB-Co (**a**) and PPy-Co (**b**) catalysts.

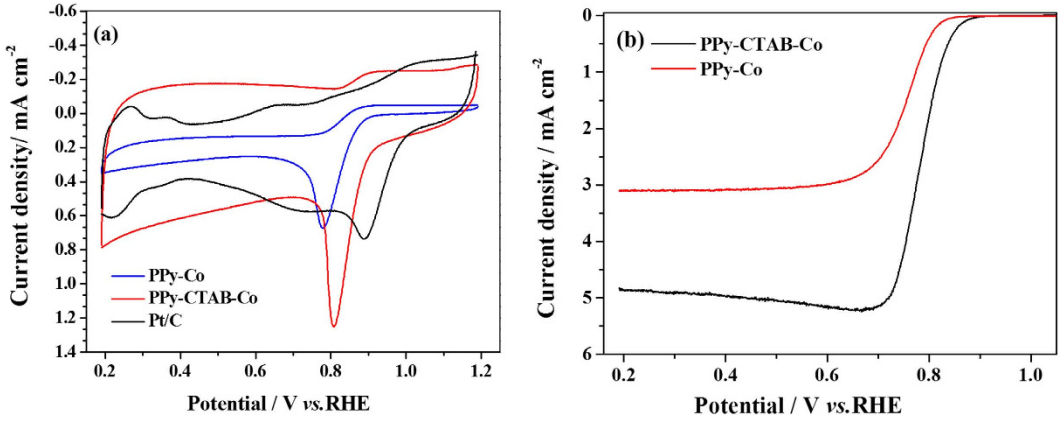

Figure 3. Cyclic voltammograms (CVs) (**a**), and I-V polarization curves at 1600 rpm (**b**) of PPy-CTAB-Co and PPy-Co catalyzed glassy carbon electrodes in O_2-saturated 0.1 M KOH solution. Potential scanning rates for both CVs and I-V curves are 5 mV s^{-1}; Catalyst loadings: 0.40 mg cm^{-2}.

Figure 3b presents the polarization curves of the PPy-CTAB-Co and PPy-Co catalysts measured at an electrode rotating rate of 1600 rpm with a potential scanning rate of 5 mV s^{-1}. Both the onset and half wave potentials of PPy-CTAB-Co catalyst are obviously higher than that of granular PPy-Co, indicating again the higher catalytic activity of the nanowire PPy-CTAB-Co.

To quantitatively investigate the ORR performance of the nanowire PPy-CTAB-Co catalyst, Fig. 4a gives the RDE curves measured at various electrode rotating rates along with that of PPy-Co shown in Fig. 4c for comparison. Generally, the number of transferred electrons (n), the so-called 4-electron pathway selectivity, for ORR can be calculated with Koutecky-Levich (K-L) equation[39]:

$$j^{-1} = j_k^{-1} + j_{dl}^{-1} = j_k^{-1} + (Bw^{1/2})^{-1} \quad (1)$$

$$B = 0.62nFC_0{D_0}^{2/3}{v_0}^{-1/6} \quad (2)$$

where j is the disk current density, j_k is the kinetic current density, j_{dl} is the diffusion current density, F is the Faraday constant, C_0 is the concentration of O_2 in the electrolyte, D_0 is the diffusion coefficient of O_2 in the electrolyte, v_0 is the kinetic viscosity of the electrolyte, and w is the rotating rate of the disk electrode. The K-L plots derived from the current densities at 0.65, 0.55, 0.45 and 0.35 V (*vs.* RHE) are shown in Fig. 4b,d giving the electron-transfer numbers of 3.71 and 3.35 for PPy-CTAB-Co and PPy-Co, respectively. This indicates that both the nanowire PPy-CTAB-Co and granular PPy-Co undergo 4-electron-transfer dominated ORR, but the former has higher 4-electron pathway selectivity.

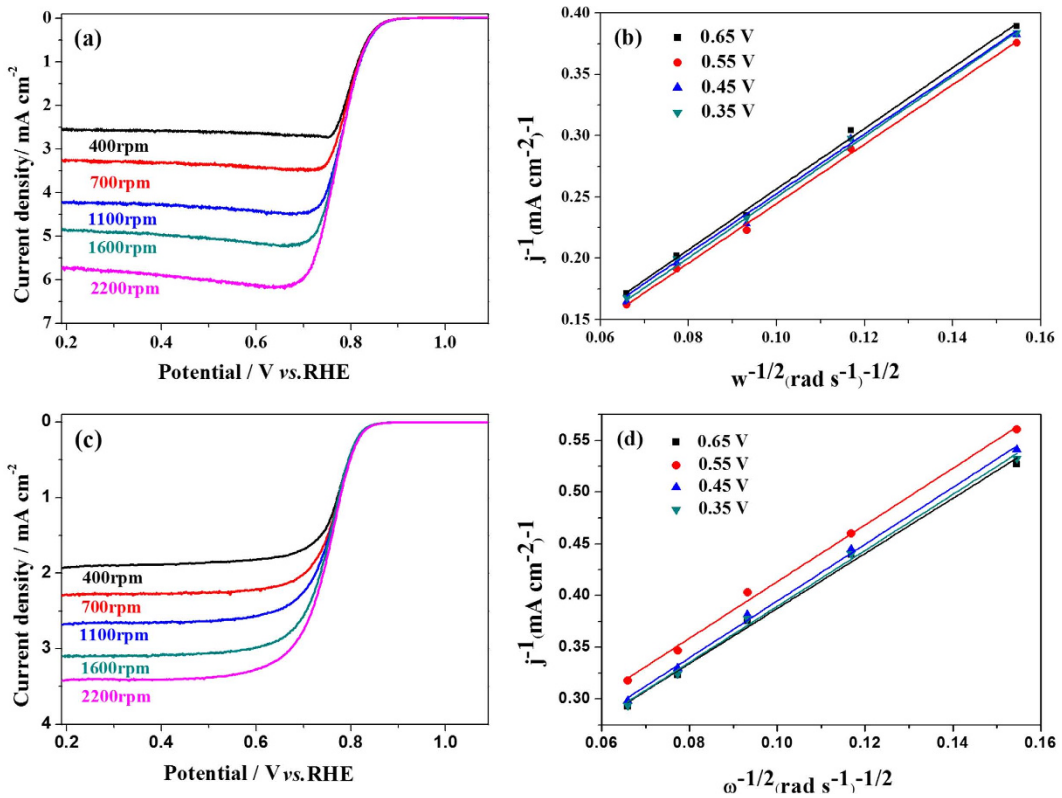

Figure 4. RDE I-V polarization curves recorded on glassy carbon electrodes coated by PPy-CTAB-Co (**a**) and PPy-Co (**c**) in O_2-saturated 0.1 M KOH solution, respectively. Potential scannig rate is 5 mV s^{-1}; Catalyst loadings: 0.40 mg cm^{-2}. K-L plots (**b,d**) of data in (**a,b**).

Stability of the catalysts. Stability is a necessary property for fuel cell catalysts. In the present work, the stability of nanowire PPy-CTAB-Co and granular PPy-Co catalysts were evaluated by comparing the CV curves in O_2-saturated 0.1 M KOH before and after 500 CV cycles in Ar-saturated 0.1 M KOH, and that of the 20 wt% Pt/C was also measured for comparison, the results are shown in Fig. 5. Excellent stability can be observed for the nanowire PPy-CTAB-Co catalyst, almost no decay could be found in its ORR peak potential, while the granular PPy-Co catalyst shows a slight decrease in ORR activity. For the commercial 20wt%Pt/C catalyst, however, its ORR peak potential is drastically decreased by 60 mV after 500 cycles. These results indicate the better stability of both PPy-CTAB-Co and PPy-Co catalysts than the 20 wt% Pt/C catalyst and the nanowire PPy-CTAB-Co catalyst can give the best stability.

Discussions

In order to understand the superior ORR performance of the nanowire PPy-CTAB-Co catalyst, diverse physiochemical characterizations were employed. Closely similar XRD patterns for PPy-CTAB-Co and PPy-Co catalysts were obtained (Fig. 6) with two broad diffraction peaks at 2θ of about 25° and 43°, which correspond to (002) and (101) phase of carbon, respectively, but none characteristic peaks for metallic cobalt or cobalt oxide could be observed in both catalysts, agreeing well with the SEM/TEM results (Figs 1 and 2) of none Co/CoO particles, probably suggesting that the Co species are not in a crystalline state. Actually the ICP measurements could detect a cobalt content of 4.356 wt% and 0.676 wt% in the catalysts of PPy-CTAB-Co and PPy-Co, respectively. XPS experiments (Fig. S1, Supporting Information) could also display surface cobalt content of 1.03 at% (PPy-CTAB-Co) and 0.24 at% (PPy-Co) in the catalysts, respectively. Consulting with our previous research[40], these results imply that the cobalt in the catalysts are bonded to nitrogen as Co-N structure, but not exist as metallic cobalt or its oxide.

Fig. S2 in Supporting Information displays the N_2 adsorption-desorption isotherm of PPy-CTAB, PPy and the resulted PPy-CTAB-Co and PPy-Co catalysts. The calculated BET surface areas for PPy-CTAB and PPy are 120 and 12 m^2 g^{-1}, respectively. This may explain why PPy-CTAB-Co catalyst has a higher cobalt content, as measured with both ICP and XPS discussed above. It is believed that the higher specific surface area of nanowire PPy-CTAB should be able to help absorbing more cobalt ions during cobalt acetate impregnation to form Co-N structure in the final catalyst[41].

N 1 s core level XPS spectra in PPy-CTAB, PPy, and the PPy-CTAB-Co and PPy-Co catalysts were captured with XPS and demonstrated in Fig. 7. In both nanowire PPy-CTAB and granular PPy, the nitrogen is dominated by a main peak of pyrrolic-N (N2) in the range from 400.1 to 400.9 eV, which can be assigned to nitrogen atoms in PPy ring. In both the catalysts of PPy-CTAB-Co and PPy-Co, however, the form of nitrogen has changed drastically because of the decomposition of PPy and structure re-configuration during high temperature pyrolysis.

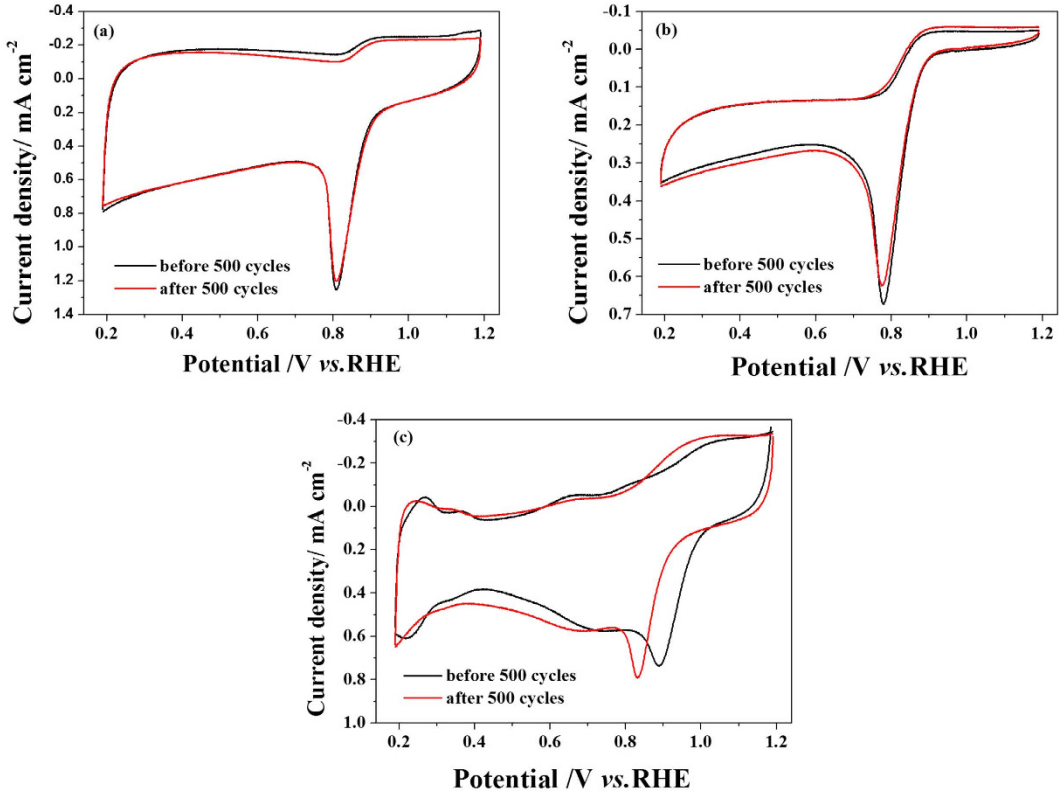

Figure 5. Stability of electrodes coated by PPy-CTAB-Co (**a**), PPy-Co (**b**) and 20wt% Pt/C (**c**), respectively, measured in O_2-saturated 0.1 M KOH solution. Potential scannig rate is 5 mV s^{-1}; Catalyst loadings: 0.40 mg cm^{-2}.

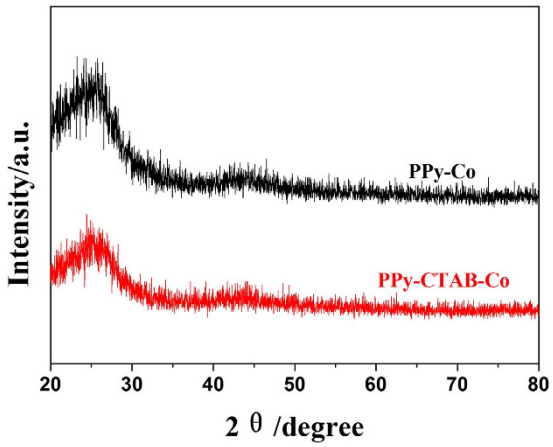

Figure 6. XRD patterns of PPy-CTAB-Co and PPy-Co catalysts.

Actually, the nitrogen in both of the catalysts could be deconvoluted into pyridinic-N (N1, 398.0–399.5 eV), pyrrolic-N (N2, 400.1–400.9 eV), quaternary-N (N3, 401–402 eV) and oxidative-N (N4, 402–410 eV)[40], as shown in Fig. 7. According to Higgins *et al.*[42], pyridinic-N could provide an edge plane exposure to readily facilitate the adsorption of oxygen, leading to improved ORR performance. Sha *et al.*[40,43] also discussed that pyridinic nitrogen could play a significant role in the ORR performance of pyrolyzed carbon supported polypyrrole-cobalt catalysts with the active sites of Co-pyridinic-N group. In this work, the evaluated concentrations of various types of nitrogen in the studied PPy-CTAB-Co and PPy-Co catalysts are listed in Table 1. It can be seen that the concentration of pyridinic-N in PPy-CTAB-Co is obviously higher than that in PPy-Co. Combined with the higher cobalt content in PPy-CTAB-Co as discussed above and the larger nitrogen content (11.38 at% compared to 8.46 at% for PPy-Co) acquired with XPS spectra (Fig. S1, Supporting Information), it is inferred that the more Co-pyridinic-N structure as ORR active sites in the nanowire PPy-CTAB-Co catalyst is a main factor responsible for the enhanced ORR performance. Moreover, the BET surface areas of PPy-CTAB-Co and PPy-Co catalysts can be calculated

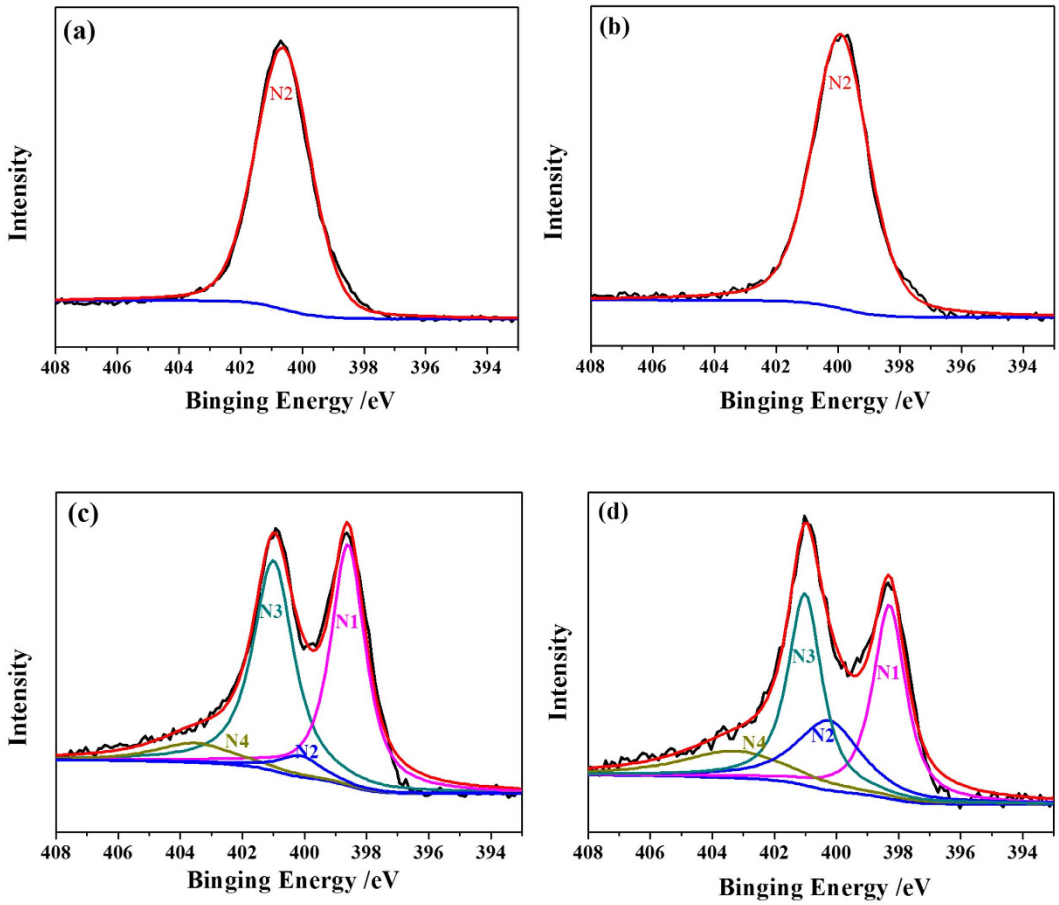

Figure 7. N 1 s XPS spectra for PPy-CTAB (**a**), PPy (**b**), PPy-CTAB-Co (**c**), and PPy-Co (**d**).

	PPy-CTAB-Co	PPy-Co
Pyridinic-N (N1)	0.4333	0.3606
Pyrollic-N (N2)	0.0464	0.0892
Quaterary-N (N3)	0.4415	0.4305
Oxidative-N (N4)	0.0788	0.1197

Table 1. Concentrations of various nitrogen groups in the catalysts of PPy-CTAB-Co and PPy-Co.

using the data in Fig. S2 (Supporting Information), which are 72.2 and 24.4 $m^2 g^{-1}$, respectively. It is another possible reason for the higher catalytic ORR activity of PPy-CTAB-Co than PPy-Co, because more Co-pyridinic-N active sites exist on the larger surface of PPy-CTAB-Co catalyst to facilitate the oxygen reduction reaction.

Conclusions

In summary, PPy-CTAB-Co catalyst with a nanowire morphology is successfully synthesized with CTAB as a surfactant and it is tested for catalyzing ORR in alkaline solution. Both much better catalytic ORR activity and higher four-electron-transfer selectivity as well as higher stability than the granular PPy-Co catalyst are observed. Although this catalyst's ORR activity is slightly inferior to that of the commercial 20 wt% Pt/C catalyst, a much better stability than the Pt/C catalyst in alkaline solution is achieved. With the help of physicochemical techniques, the enhanced ORR performance of nanowire PPy-CTAB-Co can be attributed to large quantity of Co-pyridinic-N groups as ORR active sites and its larger specific surface area which allows more active sites to expose for facilitating oxygen reduction reaction.

Methods

Synthesis of catalysts. In order to prepare nanowire PPy, cetyltrimethylammounium bromide (CTAB) was used as the surfactant. The typical procedure[44] is as follows: 1.5 mmol CTAB was stirred in 150 ml deionized water at 40 °C to form a homogeneous solution, then this solution was cooled down to 0–3 °C to form a CTAB crystalline suspension followed by the addition of pre-cooled ammonium peroxydisulfate (APS) aqueous solution (4.5 mmol APS dissolved in 25 ml deionized water). After 1 minute, 500 μl freshly distilled pyrrole was injected

and the obtained mixture was stirred for another 24 hours at 0–3 °C. The resulted mixture was washed with water and ethanol alternately for several times, and then dried under vacuum at room temperature to obtain the PPy-CTAB with a nanowire morphology.

For comparison, granular PPy with small particles was also prepared: 2 ml freshly distilled pyrrole was dissolved in 100 ml deionized water, followed by an addition of APS aqueous solution (57.6 mmol APS dissolved in 200 ml deionized water). After a stirring for 24 hours, the mixture was washed several times with water and ethanol alternately, and then dried under vacuum at room temperature to obtain the granular PPy.

In two individual experiments, 0.1 g PPy-CTAB or PPy was added into 300 ml saturated cobalt acetate solution, separately. The obtained mixture was stirred and refluxed at 60 °C for 10 hours, and then washed with excessive deionized water and dried under vacuum at 60 °C. The resulted black powders were then pyrolyzed in argon atmosphere at 800 °C for 2 hours to obtain the final catalysts of PPy-CTAB-Co and PPy-Co, respectively.

Commercial 20 wt% Pt/C catalyst from BASF company was used as the baseline for ORR performance comparison.

Characterizations. Powder XRD patterns were obtained on a Shimadzu 6000 X-ray diffract meter using Cu $K\alpha$ radiation ($\lambda = 1.5406$ Å). SEM images were recorded on a NOVA NANOSEM 450 instrument. TEM images were recorded on a JEOL JEM-2100 instrument operating at 200 kV and 30 mA. XPS measurements were performed on Kratos AXIS ULTRA DLD with Al $K\alpha$ as excitation source ($h\nu = 14$ kV). The N_2 adsorption-desorption isotherms were measured using Micromeritics ASAP 2010 M + C instrument at 77 K to calculate the Brunauer-Emmett-Telley (BET) specific surface areas. Cobalt content in the catalysts was detected using a Thermal iCAP 6000 ICP spectrometer by soaking the catalysts in aqua regia.

Electrochemical measurements. The electrochemical activities of the catalysts towards ORR were evaluated in a three-electrode cell controlled by a CHI 750 A potentiostat/galvanostat. A platinum wire and a saturated calomel electrode (SCE) were used as the counter electrode and reference electrode, respectively. A rotating disk electrode employing a glassy carbon disk ($\varnothing = 4$ mm) was used as the working electrode. 0.1 M KOH was the electrolyte.

The catalyst layer on the working electrode was prepared by pipetting 10 μl catalyst ink onto the glassy carbon disk and dried at room temperature. For catalyst ink preparation, 5.0 mg catalyst sample was ultrasonically dispersed in a solution containing 50 μl Nafion® solution (5 wt%, DuPont) and 950 μl deionized water.

Cyclic voltammograms (CVs) of the catalysts were recorded between 0.19 and 1.19 V (*vs.* RHE) in O_2-saturated 0.1 M KOH at 25 °C with a potential scanning rate of 5 mV s^{-1}. The rotating disk electrode (RDE) experiments were carried out in an alkali O_2- and Ar-saturated solution (0.1 M KOH), respectively, with the same conditions as CV at various electrode rotating rates.

References

1. Proietti, E. *et al.* Iron-based cathode catalyst with enhanced power density in polymer electrolyte membrane fuel cells. *Nat. Commum.* **2,** 416 (2011).
2. Murata, S., Imanishi, M., Hasegawa, S. & Namba, R. Vertically aligned carbon nanotube electrodes for high current density operating proton exchange membrane fuel cells. *J. Power Sources* **253,** 104–113 (2014).
3. Kim, O. H. *et al.* Ordered macroporous platinum electrode and enhanced mass transfer in fuel cells using inverse opal structure. *Nat. Commum.* **4,** 2473 (2013).
4. Shi, J., Xu, H., Zhao, H., Lu, L. & Wu, X. Preparation of $Nd_2Fe_{14}B$/C magnetic powder and its application in proton exchange membrane fuel cells. *J. Power Sources* **252,** 189–199 (2014).
5. Varcoe, J. R., Slade, R. C. & Yee, E. L. H. An alkaline polymer electrochemical interface: a breakthrough in application of alkaline anion-exchange membranes in fuel cells. *Chem. Commun.* **13,** 1428–1429 (2006).
6. Bidault, F., Brett, D. J. L., Middleton, P. H., Abson, N. & Brandon, N. P. A new application for nickel foam in alkaline fuel cells. *Int. J. Hydrogen Energy* **34,** 6799–6808 (2009).
7. Lin, B. Y. S., Kirk, D. W. & Thorpe, S. J. Performance of alkaline fuel cells: A possible future energy system? *J. Power Sources* **161,** 474–483 (2006).
8. Elzing, A., Putten, A. van der, Visscher, W. & Barendrecht, E. The cathodic reduction of oxygen at cobalt phthalocyanine: Influence of electrode preparation on electrocatalysis. *J. Electroanal. Chem. Interfa. Electrochem.* **200,** 313–322 (1986).
9. Sarangapani, S., Lessner, P., Manoukian, M. & Giner, J. Non-noble electrocatalysts for alkaline fuel cells. *J. Power Sources* **29,** 437–442 (2009).
10. Kiros, Y., Lindström, O. & Kaimakis, T. Cobalt and cobalt-based macrocycle blacks as oxygen-reduction catalysts in alkaline fuel cells. *J. Power Sources* **45,** 219–227 (1993).
11. Calegaro, M. L., Lima, F. H. B. & Ticianelli, E. A. Oxygen reduction reaction on nanosized manganese oxide particles dispersed on carbon in alkaline solutions. *J. Power Sources* **158,** 735–739 (2006).
12. Lima, F. H. B., Calegaro, M. L. & Ticianelli, E. A. Investigations of the catalytic properties of manganese oxides for the oxygen reduction reaction in alkaline media. *J. Electroanal. Chem.* **590,** 152–160 (2006).
13. Roche, I., Chaînet, E., Chatenet, M. & Vondrák, J. Carbon-Supported manganese oxide nanoparticles as electrocatalysts for the oxygen reduction reaction (ORR) in alkaline medium: Physical characterizations and ORR mechanism. *J. Phys. Chem. C* **111,** 1434–1443 (2006).
14. Pu, Z. *et al.* Spinel $ZnCo_2O_4$/N-doped carbon nanotube composite: A high active oxygen reduction reaction electrocatalyst. *J. Power Sources* **257,** 170–173 (2014).
15. Ortiz, J. & Gautier, J. L. Oxygen reduction on copper chromium manganites. Effect of oxide composition on the reaction mechanism in alkaline solution. *J. Electroanal. Chem.* **391,** 111–118 (1995).
16. Nissinen, T., Kiros, Y., Gasik, M. & Lampinen, M. Comparison of preparation routes of spinel catalyst for alkaline fuel cells. *Mater. Res. Bull.* **39,** 1195–1208 (2004).
17. Meng, H., Jaouen, F., Proietti, E., Lefèvre, M. & Dodelet, J.-P. pH-effect on oxygen reduction activity of Fe-based electro-catalysts. *Electrochem. Commun.* **11,** 1986–1989 (2009).
18. Asazawa, K. *et al.* A Platinum-free zero-carbon-emission easy fuelling direct hydrazine fuel cell for vehicles. *Angew. Chem.* **119,** 8170–8173 (2007).
19. Brushett, F. R. *et al.* A carbon-supported copper complex of 3,5-diamino-1,2,4-triazole as a cathode catalyst for alkaline fuel cell applications. *J. Am. Chem. Soc.* **132,** 12185–12187 (2010).

20. Hermann, V., Dutriat, D., Müller, S. & Comninellis, C. Mechanistic studies of oxygen reduction at $La_{0.6}Ca_{0.4}CoO_3$-activated carbon electrodes in a channel flow cell. *Electrochim. Acta* **46,** 365–372 (2000).
21. Miyazaki, K. *et al.* Single-step synthesis of nano-sized perovskite-type oxide/carbon nanotube composites and their electrocatalytic oxygen-reduction activities. *J. Mater. Chem.* **21,** 1913–1917 (2011).
22. Manoharan, R. & Shukla, A. K. Oxides supported carbon air-electrodes for alkaline solution power devices. *Electrochim. Acta* **30,** 205–209 (1985).
23. Gong, K. P., Du, F., Xia, Z. H., Durstock, M. & Dai, L. M. Nitrogen-doped carbon nanotube arrays with high electrocatalytic activity for oxygen reduction. *Science* **323,** 760–764 (2009).
24. Zheng, Y., Jiao, Y., Ge, L., Jaroniec, M. & Qiao, S. Z. Two-step boron and nitrogen doping in graphene for enhanced synergistic catalysis. *Angew. Chem. Int. Edit.* **52,** 3110–3116 (2013).
25. Liu, Z. *et al.* Sulfur-nitrogen co-doped three-dimensional carbon foams with hierarchical pore structures as efficient metal-free electrocatalysts for oxygen reduction reactions. *Nanoscale* **5,** 3283–3288 (2013).
26. Olson, T. S. *et al.* Anion-exchange membrane fuel cells: dual-site mechanism of oxygen reduction reaction in alkaline media on cobalt-polypyrrole electrocatalysts. *J. Phys. Chem. C* **114,** 5049–5059 (2010).
27. Bezerra, C. W. B. *et al.* A review of Fe–N/C and Co–N/C catalysts for the oxygen reduction reaction. *Electrochim. Acta* **53,** 4937–4951 (2008).
28. Shrestha, S. & Mustain, W. E. Properties of nitrogen-functionalized ordered mesoporous carbon prepared using polypyrrole precursor. *J. Electrochem. Soc.* **157,** B1665–B1672 (2010).
29. Khomenko, V. G., Barsukov, V. Z. & Katashinskii, A. S. The catalytic activity of conducting polymers toward oxygen reduction. *Electrochim. Acta* **50,** 1675–1683 (2005).
30. Yuan, X., Ding, X.-L., Wang, C.-Y. & Ma, Z.-F. Use of polypyrrole in catalysts for low temperature fuel cells. *Energy Environ. Sci.* **6,** 1105–1124 (2013).
31. Han, Y. *et al.* Fabrication of conducting polypyrrole film with microlens arrays by combination of breath figures and replica molding methods. *Polymer* **53,** 2599–2603 (2012).
32. Wang, Y., Wang, X., Yang, C., Mu, B. & Liu, P. Effect of acid blue BRL on morphology and electrochemical properties of polypyrrole nanomaterials. *Powder Technol.* **235,** 901–908 (2013).
33. Velazquez, J. M., Gaikwad, A. V., Rout, T. K., Rzayev, J. & Banerjee, S. A substrate-integrated and scalable templated approach based on rusted steel for the fabrication of polypyrrole nanotube arrays. *ACS Appl. Mater. Inter.* **3,** 1238–1244 (2011).
34. Ru, X. *et al.* Synthesis of polypyrrole nanowire network with high adenosine triphosphate release efficiency. *Electrochim. Acta* **56,** 9887–9892 (2011).
35. Rahman, A. & Sanyal, M. K. Novel switching transition of resistance observed in conducting polymer nanowires. *Adv. Mater.* **19,** 3956–3960 (2007).
36. Yang, Y., Liu, J. & Wan, M. Self-assembled conducting polypyrrole micro/nanotubes. *Nanotechnology* **13,** 771–773 (2002).
37. Qu, L. & Shi, G. Hollow microstructures of polypyrrole doped by poly(styrene sulfonic acid). *J. Polym. Sci. Pol. Chem.* **42,** 3170–3177 (2004).
38. Morozan, A., Jégou, P., Campidelli, S., Palacin, S. & Jousselme, B. Relationship between polypyrrole morphology and electrochemical activity towards oxygen reduction reaction. *Chem. Commun.* **48,** 4627–4629 (2012).
39. Qiao, J. *et al.* Using pyridine as nitrogen-rich precursor to synthesize Co-N-S/C non-noble metal electrocatalysts for oxygen reduction reaction. *Appl. Catal. B: Environ.* **125,** 197–205 (2012).
40. Sha, H.-D. *et al.* Experimental identification of the active sites in pyrolyzed carbon-supported cobalt-polypyrrole-4-toluenesulfinic acid as electrocatalysts for oxygen reduction reaction. *J. Power Sources* **255,** 76–84 (2014).
41. Xu, P. *et al.* Synthesis and characterization of nanostructured polypyrroles: Morphology-dependent electrochemical responses and chemical deposition of Au nanoparticles. *Polymer* **50,** 2624–2629 (2009).
42. Higgins, D. C., Meza, D. & Chen, Z. Nitrogen-doped carbon nanotubes as platinum catalyst supports for oxygen reduction reaction in proton exchange membrane fuel cells. *J. Phys. Chem. C* **114,** 21982–21988 (2010).
43. Sha, H. D. *et al.* Effects of pyrrole polymerizing oxidant on the properties of pyrolysed carbon-supported cobalt-polypyrrole as electrocatalysts for oxygen reduction reaction. *J. Electrochem. Soc.* **160,** F507–F513 (2013).
44. Wang, Y. *et al.* Synthesis of ordered spiral and ring-like polypyrrole nanowires in cetyltrimethylammounium bromide crystalline suspension. *Colloid Polym. Sci.* **287,** 1325–1330 (2009).

Acknowledgements

The authors are grateful for the financial support of this work by the National Natural Science Foundation of China (21176155 and 21476138).

Author Contributions

L.L., X.Y., D.P.W. and J.Z. designed the experiments, L.L., X.Y., Z.M., X.Y., X.W., Z.F. M. and L.Z. carried out the experiments and analysis, L.L., X.Y., D.P. W. and J.Z. wrote the paper. All authors reviewed the manuscript.

Additional Information

Supplementary information accompanies this paper at http://www.nature.com/srep

Competing financial interests: The authors declare no competing financial interests.

How to cite this article: Yuan, X. *et al.* Novel nanowire-structured polypyrrole-cobalt composite as efficient catalyst for oxygen reduction reaction. *Sci. Rep.* **6**, 20005; doi: 10.1038/srep20005 (2016).